BLOCK SHEAR FAILURES OF BOLTED CONNECTIONS

Lip H. Teh
School of Civil, Mining and Environmental Engineering, University of Wollongong, Australia
lteh@uow.edu.au

Drew D. A. Clements
Hatch, 25 Atchinson Street, Wollongong, Australia
dclements@hatch.com.au

ABSTRACT

This paper examines the mechanisms for block shear failures of bolted connections in steel plates postulated in the code equations. It explains that there is only one feasible mechanism for the limit state of conventional block shear failure, that which involves shear yielding and tensile rupture. It is shown through nonlinear contact finite element analysis that the shear failure planes are neither the gross nor the net shear planes assumed in the code equations. The paper proposes an equation that provides more accurate results compared to the code equations in predicting the block shear capacities of bolted connections in steel sheets having minimal strain hardening.

1. INTRODUCTION

Block shear failure is recognised as a strength limit state of bolted connections in the AISC Specification for Structural Steel Buildings (AISC 2010), Eurocode 3 Part 1.8 (ECS 2005) and AS/NZS 4600:2005 Cold-formed Steel Structures (SA/SNZ 2005). However, since it was discovered by Birkemoe & Gilmor (1978) and first incorporated into the AISC specification (AISC 1978), the design provision for determining the block shear capacity of a bolted connection has continued to change and even oscillate between certain equations, as described by Teh & Clements (2012). The reasons are at least two folds.

The first reason is that there was the uncertainty concerning the possible mechanisms for block shear failures. Some versions of the AISC specification (AISC 1978, 1989) implicitly assume the simultaneous shear and tensile rupture mechanism, while others provide for the shear yielding and tensile rupture mechanism and the shear rupture and tensile yielding mechanism (AISC 1986, 1993). The latest version provides for the simultaneous shear and tensile rupture mechanism and the shear yielding and tensile rupture mechanism (AISC 2010).

The second reason is the inconsistent definitions of the shear failure planes used in the code equations for determining the block shear capacity. The gross shear area is used when the failure mechanism is shear yielding and tensile rupture, while the net shear area is used for the supposed shear rupture and tensile yielding mechanism or simultaneous shear and tensile rupture mechanism.

This paper describes the research results of the authors that resolve the perennial questions regarding the feasible mechanism for block shear failures of bolted connections and the location of the shear failure planes.

2. FEASIBLE MECHANISM FOR BLOCK SHEAR FAILURES

Consider the connected end of a flat member shown in Figure 1 that is subjected to a concentric load and is restrained from out-of-plane failure modes. Leaving out the pure net section tension failure mode and the bearing failure mode from the present discussion, there are essentially only two possible failure modes for the connected end. If the connection shear length (which is denoted by e_n in Figure 1) is relatively short, it will fail by "shear out" of each bolt.

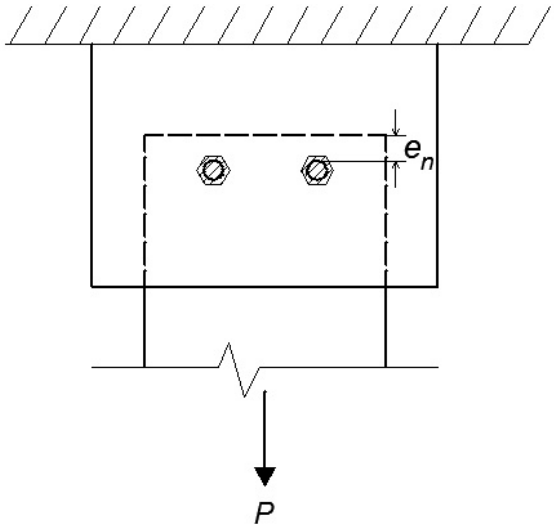

Figure 1. A two-bolt connection

As the connection shear length e_n increases, or as the bolt spacing decreases, or both, any of which results in an increase of the aspect ratio, a condition would be reached such that it is conceivable for the connected end to undergo block shear failure by simultaneous shear and tensile ruptures. The aspect ratio at which the hypothetical mechanism of simultaneous shear and tensile ruptures could occur is termed the threshold ratio in the present work.

However, once yielding around the perimeter of the block takes place and the block displaces as a whole, the tensile strains in the net section between bolt holes increase much more rapidly than the shear strains so that the block eventually fails by shear yielding and tensile rupture. Even at an aspect ratio that is slightly lower than the threshold ratio, a block shear failure by shear yielding and tensile rupture is still possible as shown in Figure 2, where the shear-out deformations were over-run by the shear yielding and tensile rupture mechanism. The change-over in the failure mode took place when yielding started in the tensile net section between the two bolt holes, where tensile rupture eventually took place.

Figure 2. Shear-out deformations gave way to block shear failure

As the aspect ratio increases beyond the threshold ratio, block shear failure can only be due to shear yielding and tensile rupture since the tensile strains are always more critical than the shear strains.

Obviously, at an aspect ratio that is sufficiently lower than the threshold ratio, the shear-out failure mode governs. There is therefore no aspect ratio at which a block shear failure occurs by the shear rupture and tensile yielding mechanism.

3. RELEVANT EQUATIONS FOR BLOCK SHEAR CAPACITY

Having established that a conventional block shear failure invariably fails by the shear yielding and tensile rupture mechanism, as borne out by laboratory test results, the present work is only concerned with the equations that are based on such a mechanism. There are three equations to consider.

The first equation is found in the AISC specification (AISC 2010) and the Australasian cold-formed steel structures standard (SA/SNZ 2005)

$$P_p = F_u A_{nt} + 0.6 F_y A_{gv} \tag{1}$$

in which F_u is the material tensile strength, F_y is the yield stress, A_{nt} is the net tensile area, and A_{gv} is the gross shear area. The implied block is depicted in Figure 3(a), which shows that the shear failure planes assumed in Equation (1) lie at the outer perimeter of the block.

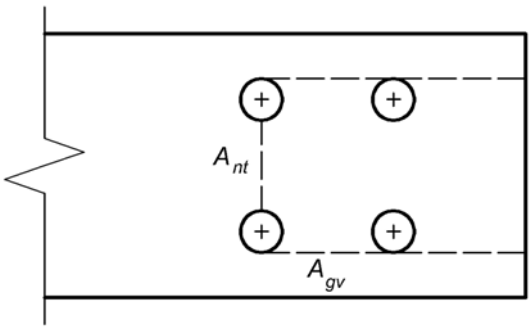

(a) Gross shear planes

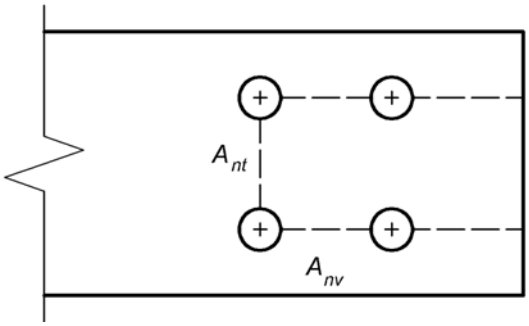

(b) Net shear planes

Figure 3. Gross and net shear failure planes

The second equation to consider is found in the European code (ECS 2005)

$$P_p = F_u A_{nt} + F_y A_{nv} / \sqrt{3} \approx F_u A_{nt} + 0.577 F_y A_{nv} \tag{2}$$

in which A_{nv} is the net shear area indicated in Figure 3(b). This approach ignores the fact that the planes coinciding with the centrelines of the bolt holes in the direction of loading do not have maximum shear stresses due to the bolt bearing condition.

The third equation was proposed by Teh & Clements (2012)

$$P_p = F_u \sum A_{nt} \left(0.9 + 0.1 d / p_2 \right) + 0.6 F_y A_{av} \tag{3}$$

in which A_{av} is the active shear area defined in Figure 4. The variable d denotes the bolt diameter while p_2 is defined in Figure 5. The active shear area has been used by Teh & Clements (2012) based partially on the experimental evidence of Franchuk et al. (2003) shown in Fig. 3 of their paper.

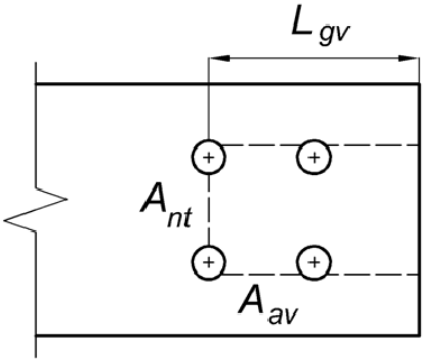

$$L_{av} = L_{gv} - \left(\frac{n_r - 1}{2} + \frac{1}{4} \right) d_h$$

$$\approx L_{gv} - n_r d_h / 2$$

$$A_{av} = 2 L_{av} t$$

Figure 4. Active shear planes

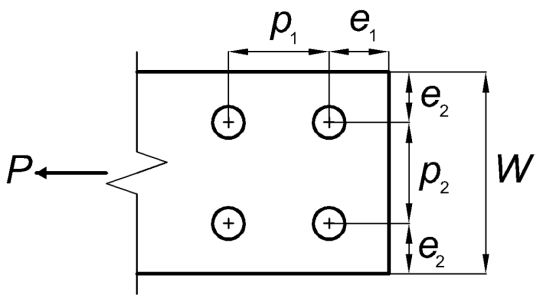

Figure 5 Definitions of geometric variables

Equation (3) incorporates an in-plane “shear lag factor” proposed by Teh & Gilbert (2012) in determining the net section tension capacity. The shear lag factor accounts for the fact that the tensile stresses are not uniformly distributed across the net section, which has a significant effect on the tension capacity of bolted connections in cold-reduced sheet steel.

4. DETERMINATION OF THE SHEAR FAILURE PLANES

In the present work, the location of the shear failure planes is determined through geometrically and materially nonlinear contact finite element analysis using ABAQUS 6.9 (ABAQUS 2009). The finite element models simulate concentrically loaded bolted connections in steel sheets, an example of which is shown in Figure 6 for a specimen with one row of bolts. It is the inner sheet subjected to double shear that was modelled in the finite element analysis.

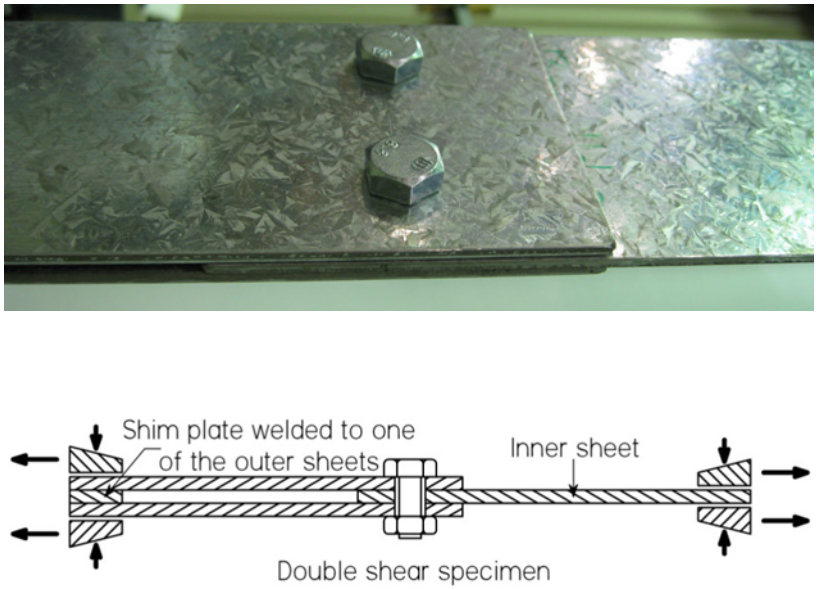

Figure 6. Concentrically loaded sheet

Due to symmetry, only half of the concentrically loaded sheet was modelled as shown in Figure 7 with transverse displacements prevented across the symmetry plane. Rotation about the symmetry axis was also prevented. The left end was completely restrained (fixed) and only the mid-plane of the sheet, indicated by the lines running along the middle of the sheet thickness, was restrained out-of-plane so that necking through the sheet thickness was not prevented. The hexahedral reduced integration brick element type C3D8R available in ABAQUS 6.9 (ABAQUS 2009) was used so that each finite element model was three dimensional. An example of the finite element mesh is shown in Figure 8.

Loading of the connection was simulated by displacing the bolt away from the fixed end as indicated by the dashed arrow in Figure 7, which would be resisted by the contact surface between the bolt and the bolt hole at the downstream end. The bolt was modelled as a 3D analytical rigid body revolved shell, and the bolt hole had a diameter that was 1 mm larger than the bolt, as was the case with the laboratory test specimens.

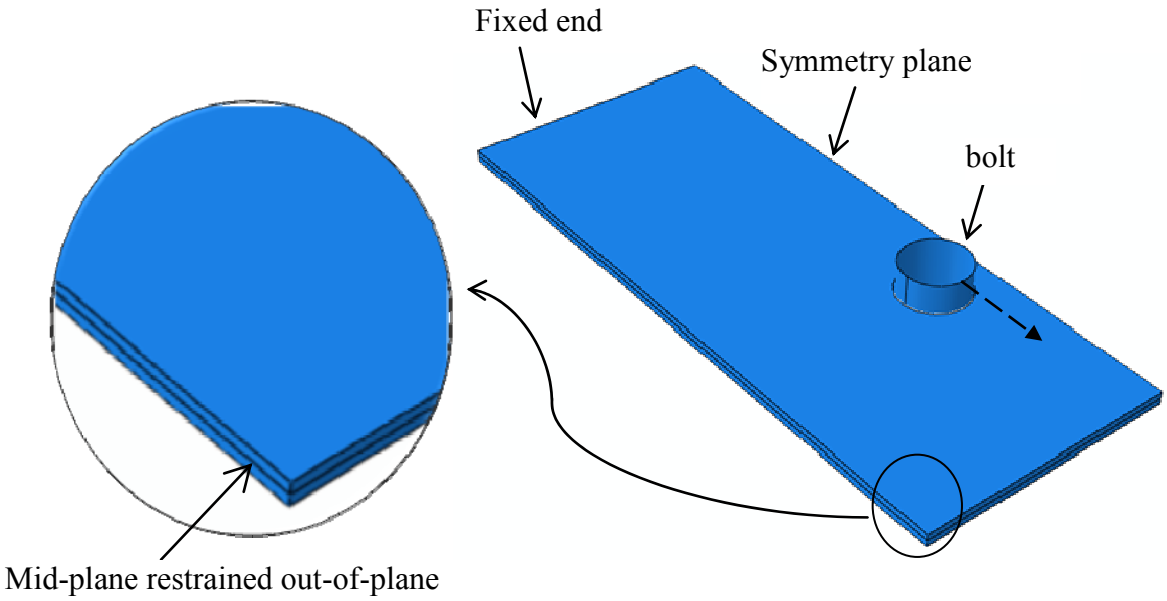

Figure 7. Conceptual model

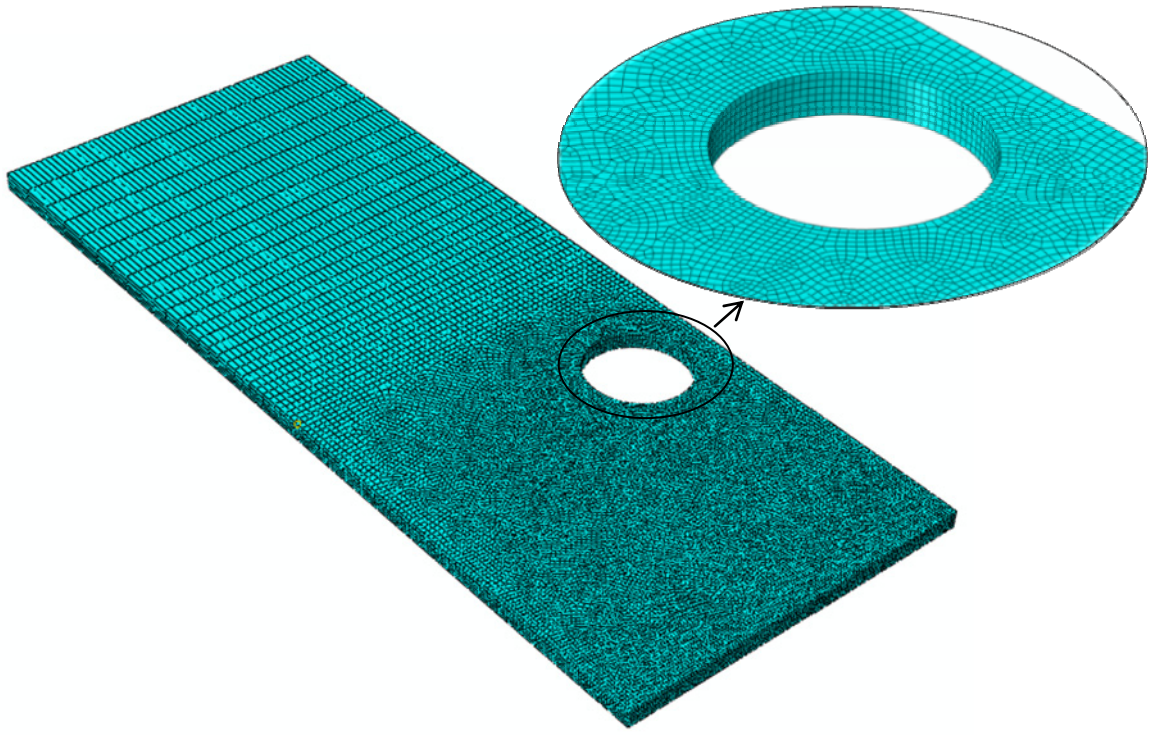

Figure 8. Finite brick element (C3D8R) mesh

Figure 9 shows the true in-plane shear stress contours of a sample specimen having one row of bolts. It can be seen that the largest shear stresses take place along a shear plane that is midway between the gross and the net shear planes indicated in Figure 3. The active shear planes depicted in Figure 4 represent the FEA results most closely.

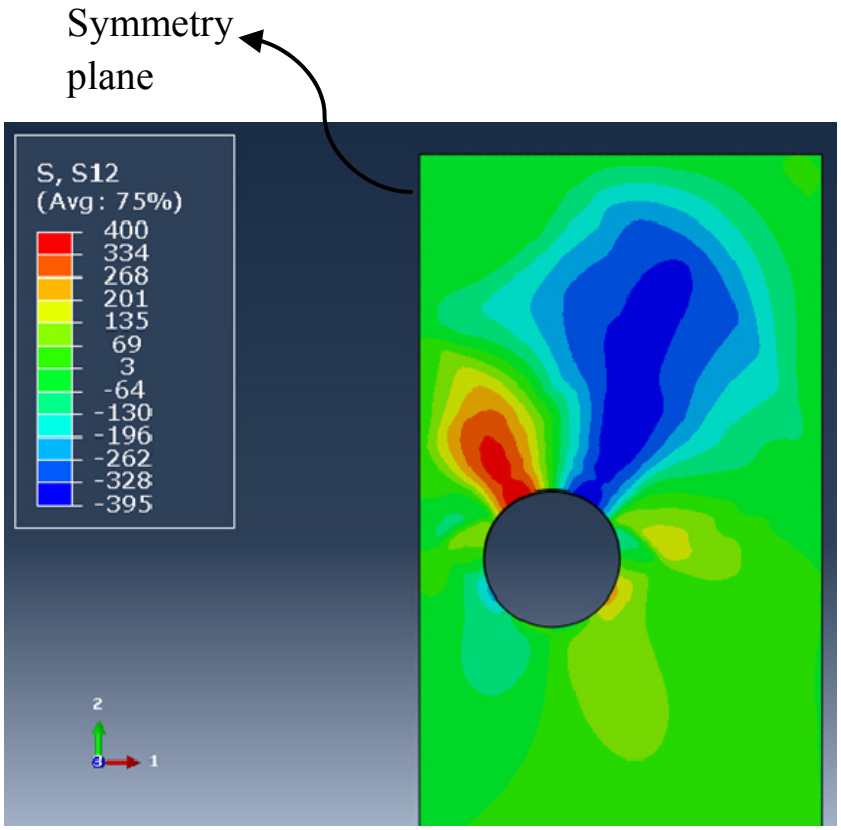

Figure 9. In-plane shear stresses of a specimen with one row of bolts

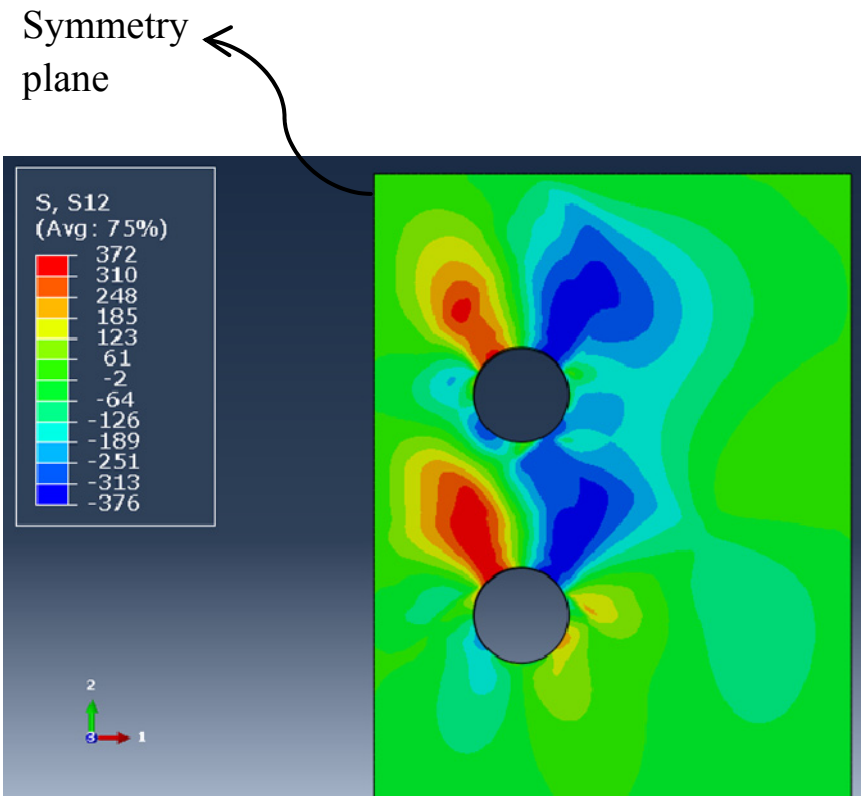

Figure 10. In-plane shear stresses of a specimen with two rows of bolts

It can also be seen that the largest shear stresses only take place within a short portion of each active shear plane, with the shear stresses approaching zero towards the downstream end. As shown in Figure 4, the active shear area A_{av} in Equation (3) is calculated by ignoring a portion of each active shear plane over a length equal to a quarter of the bolt hole diameter. This neglect is supported by the shear stress contours in Figure 9.

Figure 10 shows the true in-plane shear stress contours of a specimen with two rows of bolts. As with the previous specimen having one row of bolts only, the active shear planes are still best represented by Figure 4. The shear stress contours also support the formula for determining the active shear area A_{av} shown in Figure 4.

5. COMPARISONS OF ALTERNATIVE EQUATIONS

Tables 1 and 2 show the ratios of ultimate test load P_t to predicted failure load P_p computed using Equations (1) through (3), for specimens having one and two rows of bolts, respectively. The variable t denotes the nominal sheet thickness, the variable d_h the nominal bolt hole diameter, and all the other geometric variables are defined in Figure 5.

Table 1. Professional factors for specimens with one row of bolts

Spec	W (mm)	p_2 (mm)	t (mm)	e_1 (mm)	d_h (mm)	P_t/P_p (1)	(2)	(3)
CPD14	100	33	1.5	50	17	0.80	0.95	0.95
CPD15	100	33	3.0	50	13	0.90	1.02	1.01
CPD16	100	33	3.0	50	17	0.89	1.06	1.04
CPD18	120	40	1.5	50	17	0.86	1.01	1.00
CPD19	120	40	3.0	50	13	0.90	1.01	1.01
CPD20a	120	40	3.0	50	17	0.93	1.08	1.07
CPD20b	120	40	3.0	50	17	0.93	1.07	1.07
CPD22a	100	26	1.5	50	17	0.81	0.99	0.96
CPD22b	100	26	1.5	50	17	0.83	1.02	0.99
CPD23a	100	26	3.0	50	13	0.90	1.03	1.01
CPD23b	100	26	3.0	50	13	0.89	1.02	1.01
CPD24a	100	26	3.0	50	17	0.87	1.05	1.02
CPD24b	100	26	3.0	50	17	0.87	1.05	1.02
CPD26a	120	26	1.5	50	17	0.85	1.03	1.01
CPD26b	120	26	1.5	50	17	0.84	1.02	1.00
CPD27	120	26	3.0	50	13	0.91	1.04	1.02
CPD28a	120	26	3.0	50	17	0.91	1.09	1.06
CPD28b	120	26	3.0	50	17	0.89	1.07	1.04
CPD36	130	45	3.0	30	17	0.94	1.11	1.13
					Mean	0.88	1.04	1.02
					COV	0.044	0.038	0.041

The engineering properties substituted into the equations are given in Table 3, which lists the average base metal thicknesses t_{base}, yield stresses F_y, tensile strengths F_u and elongations at fracture over 15 mm, 25 mm and 50 mm gauge lengths ε_{15}, ε_{25} and ε_{50}, and uniform elongation outside fracture ε_{uo} of the 1.5-mm and 3.0-mm G450 sheet steels used to fabricate the test specimens.

Table 2. Professional factors for specimens with two rows of bolts (p_1 = 30 mm)

Spec	W (mm)	p_2 (mm)	t (mm)	e_1 (mm)	d_h (mm)	P_t/P_p (1)	(2)	(3)
CQ2a	120	26	1.5	50	17	0.73	1.08	0.92
CQ2b	120	26	1.5	50	17	0.74	1.09	0.93
CQ3	120	26	3.0	50	13	0.85	1.12	1.00
CQ4	120	26	3.0	50	17	0.80	1.15	0.99
CQ5a	130	40	1.5	30	13	0.82	1.10	0.99
CQ5b	130	40	1.5	30	13	0.81	1.08	0.98
CQ6a	130	40	1.5	30	17	0.77	1.14	0.98
CQ6b	130	40	1.5	30	17	0.77	1.14	0.99
CQ7	130	40	3.0	30	13	0.89	1.17	1.07
CQ8	130	40	3.0	30	17	0.83	1.22	1.06
CQ9b	130	55	1.5	30	13	0.81	1.04	0.97
CQ10a	130	55	1.5	30	17	0.78	1.08	0.98
CQ10b	130	55	1.5	30	17	0.80	1.10	1.00
CQ11	130	55	3.0	30	13	0.87	1.09	1.03
CQ12	130	55	3.0	30	17	0.85	1.17	1.06
					Mean	0.81	1.12	1.00
					COV	0.055	0.042	0.044

Table 3. Measured engineering properties

	t_{base} (mm)	F_y (MPa)	F_u (MPa)	F_u / F_y	ε_{15} (%)	ε_{25} (%)	ε_{50} (%)	ε_{uo} (%)
1.5 mm	1.48	605	630	1.04	21.3	18.0	12.0	6.8
3.0 mm	2.95	530	580	1.09	29.3	22.0	15.3	8.1

The use of the present steel materials, which have low ratios of tensile strength F_u to yield stress F_y, means that the "noise" due to significant shear strain hardening that had clouded the previous evaluations of alternative equations, discussed by Teh & Clements (2012), is now minimal.

It can be seen from Tables 1 and 2 that only Equation (3) provides consistent accuracy for the tested specimens. Equation (1) is over-optimistic while Equation (2) is too conservative for the specimens having multiple rows of bolts.

5. CONCLUSIONS AND GENERAL RECOMMENDATIONS

Among the various mechanisms for conventional block shear failures postulated in the literature and anticipated in the design codes, there is only one feasible mechanism, that which involves shear yielding and tensile rupture. The physical reasoning presented by the authors explains why extensive published laboratory tests have never found a block shear failure caused by any other mechanisms anticipated in the steel design codes around the world.

The authors used geometrically and materially nonlinear contact finite element analysis to confirm that the active shear planes lie between the gross and the net shear planes, as indicated by the experimental evidence obtained by other researchers. The finite element analysis results also show that the in-plane shear stresses approach zero towards the downstream end of the connection. The active shear area so defined is required for an accurate determination of the block shear capacity of a bolted connection.

The equation proposed by the authors, which is based on the shear yielding and tensile rupture mechanism, and which makes use of the active shear area, has been demonstrated to provide the most consistent and accurate results in predicting the block shear capacities of the tested specimens.

The equation representing the shear yielding and tensile rupture mechanism given in the AISC specification and the Australasian cold-formed steel structures standard significantly overestimate the block shear capacities of all specimens tested in the present work. The major reason is the use of the gross area in computing the shear yielding resistance component of the block shear capacity.

The equation specified in the current European steel structures code significantly underestimates the block shear capacities of the double-row bolted connection specimens. The conservatism is due to the use of an over-reduced shear area, and increases with increasing number of bolt rows as the difference between the net and the active shear areas widens while the shear resistance becomes more important relative to the tensile resistance.

Other code equations representing the shear rupture and tensile yielding mechanism or the simultaneous shear and tensile rupture mechanism have been previously shown by the authors to lead to unconservative results. In any case, such equations should not be used as they represent non-existent failure mechanisms.

The block shear capacity of a bolted connection in steel plates can and should be estimated based on the shear yielding and tensile rupture mechanism in conjunction with the active shear planes that lie between the gross and the net shear planes.

REFERENCES

ABAQUS (2009) ABAQUS Analysis User's Manual, Version 6.9, Dassault Systèmes, Providence RI.

AISC (1978) Specification for the Design, Fabrication and Erection of Structural Steel for Buildings, American Institute of Steel Construction, Chicago IL.

AISC (1986) Load and Resistance Factor Design Specification for Structural Steel Buildings, American Institute of Steel Construction, Chicago IL.

AISC (1989) Allowable Stress Design Specification for Structural Steel Buildings, American Institute of Steel Construction, Chicago IL.

AISC (1993) Load and Resistance Factor Design Specification for Structural Steel Buildings, American Institute of Steel Construction, Chicago IL.

AISC (2010) Specification for Structural Steel Buildings, ANSI/AISC 360-10, American Institute of Steel Construction, Chicago IL.

Birkemoe, P.C., and Gilmor, M.I. (1978) "Behavior of bearing-critical double-angle beam connections." *Engineering Journal AISC*, 15 (3), 109–115.

ECS (2005) Eurocode 3: Design of steel structures, Part 1.8: Design of joints, EN 1993-1-8, European Committee for Standardisation, Brussels, Belgium.

Franchuk, C. R., Driver, R. G., and Grondin, G. Y. (2003) "Experimental investigation of block shear failure in coped steel beams." *Can. J. Civ. Eng.*, 30, 871-881.

SA/SNZ (2005) Cold-Formed Steel Structures, AS/NZS 4600:2005, Standards Australia/Standards New Zealand.

Teh, L. H., and Clements, D. D. A. (2012) "Block shear capacity of bolted connections in cold-reduced steel sheets," scheduled for publication in April 2012 in *J. Struct. Eng.*, ASCE.

Teh, L. H., and Gilbert, B. P. (2012) "Net section tension capacity of bolted connections in cold-reduced steel sheets," scheduled for publication in March 2012 in *J. Struct. Eng.*, ASCE.